HHS Public Access

Author manuscript

Cancer Res. Author manuscript; available in PMC 2017 December 15.

Published in final edited form as:

Cancer Res. 2016 December 15; 76(24): 7208–7218. doi:10.1158/0008-5472.CAN-16-1681.

A hyaluronidase responsive nanoparticle-based drug delivery system for targeting colon cancer cells

Mingzhen Zhang[1,2,*], **Changlong Xu**[1,2,5], **Liuqing Wen**[4], **Moon Kwon Han**[1,2], **Bo Xiao**[1,2], **Jun Zhou**[4], **Yuchen Zhang**[1,2], **Zhan Zhang**[1,2], **Emilie Viennois**[1,2], and **Didier Merlin**[1,2,3]

[1]Institute for Biomedical Sciences, Georgia State University, Atlanta, GA 30303, USA

[2]Center for Diagnostics and Therapeutics, Georgia State University, Atlanta, GA 30303, USA

[3]Veterans Affairs Medical Center, Decatur, GA, 30030, USA

[4]Department of Chemistry, Georgia State University, Atlanta, GA 30303, USA

[5]The 2nd Affiliated Hospital & Yuying Children's Hospital of Wenzhou Medical University, Wenzhou, Zhejiang, 325027, P. R. China

Abstract

The ability of nanoparticles to target tumors and to enable site-specific drug release provides a unique system for the delivery of effective therapy with reduced toxic side effects. In this study, we used mesoporous silica nanoparticles (MSN) to fabricate a targeted drug delivery system that is responsive to hyaluronidase (HAase). Following engraftment of desthiobiotin onto the surface of MSN, a streptavidin complex was generated which was functionalized with biotin-modified hyaluronic acid (HA) to enable controlled drug release at cancer cells expressing HAase. Various technologies were used to confirm the successful fabrication of this MSN-based nanocarrier system for targeted drug delivery. *In vitro* analyses showed that the release of doxorubicin hydrochloride (Dox) was accelerated significantly in the presence of biotin or HAase and accelerated further in the presence of biotin and HAase. Uptake by cancer cells was mediated efficiently by CD44-receptor mediated endocytosis and that the MSN exhibited good biocompatibility *in vitro* and *in vivo*. MSN-HA/Dox nanoparticles induced apoptosis in cancer cells more efficiently than free Dox and inhibited tumor growth with minimal systemic toxicity *in vivo*. Collectively, our findings offered a preclinical proof of concept for a novel targeted drug delivery carrier system for cancer therapy.

Keywords

Mesoporous silica nanoparticle; Biotin/HAase dual stimulation; Targeted drug delivery system; Nanomedicine; Colon Cancer

[*]Author for correspondence: Tel.: +1 (404) 413 3597; Fax: +1 (404) 413 3580, mzhang21@gsu.edu; mingzhang20140215@gmail.com.

Confliction of Interest: The authors declare no conflict of interest.

Introduction

Malignant tumors are worldwide threats to human health (1). The traditional anticancer strategies, such as chemotherapy, do not distinguish cancerous cells from the healthy cells, and thus may have poor therapeutic effect on tumors while inflicting collateral damage to healthy cells (2). To address this formidable challenge, diverse classes of nanotechnology-based drug delivery systems (DDS) have been designed. These efforts have shown great promise for improving cancer treatment. The reported DDS have involved polymeric nanoparticles (3), liposomes (4), dendrimers (5), inorganic nanoparticles (6), and protein nanoparticles (7). Some of these delivery vehicles take advantage of the enhanced permeability and retention (EPR) effect, through which drugs passively accumulate in tumors due to the leakiness of the vasculature surrounding the mass (8). However, this passive approach is limited by it's over dependence on the degree of tumor vascularization and angiogenesis (9, 10), and the high interstitial fluid pressure of solid tumors can work against the successful uptake and homogenous distribution of the drug (10).

As an alternative strategy, researchers have modified delivery vehicles with targeting ligands, such as polysaccharides, antibodies, proteins, and aptamers (6), which should enable active targeting ability via binding to cognate receptors that are overexpressed by cancer cells or angiogenic endothelial cells (11). In this approach, a targeting moiety attached to the surface of DSS may act as a homing device, thereby improving the selective delivery of the loaded drug to specific tissues/cells. In addition to targeting, a DDS should enable the controlled release of drug molecules with a proper behavior to achieve an effective local concentration (12). However, entrapped drug molecules often leak from the delivery vehicles upon their introduction to aqueous solution. To maximize cancer cell death and minimize metastatic spread, a DDS should therefore combine cancer cell targeting with controlled intracellular drug release (13).

Among the reported DDS, mesoporous silica nanoparticles (MSN) have emerged as robust vehicles for drug delivery. MSN have many unique and beneficial properties, including well-defined pore structures, excellent biocompatibility, a tunable pore size, and an easily functionalized surface (14, 15). Moreover, the same MSN surface can be simultaneously assembled with multiple different moieties, such as a stimulus-responsive moiety and a targeting moiety. Many stimulus-responsive MSN based DDS have been designed to respond to various internal and external stimuli, such as pH (16), redox status (14, 15), enzyme activity (17), small molecules (18), light (19), and temperature (20).

Hyaluronic acid (HA) has recently been highlighted as a tumor-targeting moiety. It is composed of *N*-acetylglucosamine and *D*-glucuronic acid disaccharide units, and is generally considered to be a non-toxic and biodegradable natural acidic polysaccharide macromolecule (21). CD44, the cluster of differentiation (CD) protein, is the main HA-binding receptor. This single-chain transmembrane glycoprotein has a molecular mass of 80–250 kDa and is reportedly overexpressed on various tumor cells, including those of ovarian, breast, and colon cancers (22). In addition to its targeting ability, HA has other unique properties, including its large and biocompatible molecular size, which can be used to block the release of a drug, and its ability to be readily degraded to lower-molecular-

weight components by HAase after being taken up by cancer cells through receptor-mediated endocytosis (forming the basis for enzyme-responsive release).

Vitamin H, or more commonly known as biotin, is a B-complex vitamin that helps the body convert food (carbohydrates) into a fuel (glucose) used to produce energy. Biotin also helps the body metabolize fats and protein, and can generally promote cell growth (23). However, recent work suggested that biotin may be upregulated in some cancer tissues (*e.g.*, colon cancers) compared to normal tissues (24). Desthiobiotin is a modified form of biotin that binds less tightly to SA than biotin, while still exhibiting excellent binding specificity [dissociation constant (K_d) = 10^{-11} M and 10^{-15} M, respectively] (25). We hypothesized that the affinities of desthiobiotin and biotin toward SA could be combined with the targeting ability and HAase-mediated degradation of HA to develop a new MSN-based DDS that exhibits targeted drug delivery and intracellular dual-stimulus-responsive drug release.

Here, we report a novel multifunctional MSN-based biotin/HAase dual-stimulus-triggered DDS for targeted therapeutic drug delivery *in vitro* and *in vivo*. Doxorubicin hydrochloride (Dox) was investigated as a model anti-cancer drug. In this system, desthiobiotin-SA complex and HA were employed as ‘gatekeepers’. Briefly, the external surface of each MSN was modified with desthiobiotin molecules; the MSN pores were blocked with SA *via* the desthiobiotin-SA interaction; and biotin-modified HA was added to further block the pores and endow MSN-HA/Dox with its targeting capability (Figure 1A). We propose that after MSN-HA/Dox is preferentially taken up by cancer cells through receptor-mediated endocytosis, the HAase-mediated degradation of HA triggers drug release that undergoes further enhancement by the displacement of desthiobiotin by intracellular biotin (Figure 1B). This targeted drug release induces cell apoptosis and inhibits tumor growth *in vivo*. Our results suggest that the developed MSN may potentially be a promising drug delivery carrier for efficient tumor therapy.

Materials and Methods

Synthesis of desthiobiotin-functionalized mesoporous silica nanoparticles (MSN-desthiobiotin)

For MSN-desthiobiotin synthesis, 110 mg propylamine functionalized silica (MSN-NH_2) was dispersed in 10 ml PBS (pH 7.4). Then, 20 mg NHS-desthiobiotin dissolved in 1ml DMSO was added and stirred (1000 rpm) at room temperature overnight. The mixture was washed with PBS for three times and dried using lyophilizer to yield the desthiobiotin functionalized MSN (MSN-desthiobiotin).

Synthesis of SA functionalized mesoporous silica nanoparticles (MSN-SA)

For MSN-SA synthesis, 10 mg MSN-desthiobiotin was dispersed in 4 ml PBS (pH 7.4). Then, 1 ml SA (1 mg/ml in PBS) was added and allowed to react at room temperature for 2 h. The mixture was washed with PBS for three times and dried using lyophilizer to yield the SA functionalized MSN (MSN-SA).

Preparation of MSN-HA drug delivery system

The MSN-desthiobiotin (10 mg, 4 ml in PBS) was added to 5 ml of Dox (1 mg/ml) in PBS (pH 7.4) solution. After stirring about 12 h, 1 ml SA (1 mg/ml in PBS) was added and allowed to react at room temperature for 2 h to cap the pores on the mesoporous silica particles. The final mix solution was centrifuged and washed with PBS for three times, the amount of Dox loaded into MSN-desthiobiotin was determined by analyzing the absorbance of supernatant solution. Rhodamine B was loaded by the same protocol. Then, MSN-SA (2.5 ml, 2mg/ml) was redispersed in PBS, and mono-biotin labeled hyaluronan (HA) (2mg in 200 μl PBS) was added to incubate for another 2 h to obtain hyaluronic acid modified MSN (MSN-HA), The theoretical capping amount of HA on the surface of MSN was 15 μg/mg MSN.

Cell culture

Macrophage 264.7, HT-29 and Colon 26 cells were cultured to confluency in 75-cm^2 flasks at 37°C in a humidified atmosphere containing 5 % CO_2. HT-29 Cell were cultured in McCoy's 5A medium, Macrophage 264.7 cells were cultured in Dulbecco's Modified Eagle Medium (DMEM), and Colon 26 cells were culture in RPMI 1640 medium (Life Technologies, NY, USA). All these cases were supplemented with penicillin (100 U/ml), streptomycin (100 U/ml), and heat-inactivated fetal bovine serum (10 %) (Atlanta Biologicals, GA, USA). All these cell lines were obtained directly from ATCC (2009–2013) where they were tested and authenticated via morphology, and PCR to rule out interspecies and intraspecies contamination.

Animals

Athymic BALB/c nu/nu female mice, C57BL/6 and FVB/NJ female mice (6–8 wk old) were purchased from Jackson Laboratories (Bar Harbor, ME, USA). Mice were housed under specific pathogen-free conditions. All the experiments involving mice were approved by the Institutional Animal Care and Use Committee (IACUC) of Georgia State University (Atlanta, GA, USA).

Statistical analysis

One-way and two-way analyses of variance (ANOVA) and *t*-tests were used to determine statistical significance (*p<0.05, **p<0.01, ***p<0.001).

Results and Discussion

Preparation and characterization of MSN-HA drug delivery syestem

Propylamine functionalized MSN (MSN-NH_2) (~ 180 nm in diameter) was characterized by a typical hexagonal channel-like mesoporous structure, as confirmed by scanning electron microscope (SEM), transmission electron microscope (TEM), small-angle X-ray diffraction (Figure 2A–C), and nitrogen adsorption-desorption isotherms (Figure S1). Consistent with previous reports (26, 27), MSN-NH_2 displayed a homogeneous spherical morphology and had a highly regular mesoporous structure. Investigation confirmed that nanoparticles < 200 nm in diameter can circulate in blood for an extended period (28), thus the characteristics of

our developed MSN suggest that they could potentially reach the target *via* circulation and might be useful carriers for drug delivery.

To construct our MSN-HA DDS, we first conjugated MSN-NH_2 with NHS-activated desthiobiotin molecules, which are known to react efficiently with primary amine groups (-NH_2), such as those on the surface of MSN-NH_2, to form stable amide bonds (23). The efficient conjugation of desthiobiotin with MSN (MSN-desthiobiotin) was validated by the appearance of a broad absorption band at around 1680 cm^{-1} in the Fourier Transform Infrared (FITR) spectra (Figure S2), which can be assigned to vibrations of the cyclic urea group within the attached desthiobiotin molecules. For some experiments, the MSN were loaded with Dox, as a model anti-cancer drug, or rhodamine B, which was used as a tracer to locate the distributions of MSN within the cells. After Dox was loaded into the pores of MSN-desthiobiotin, SA was added to cap the pores through the desthiobiotin-SA interaction. Desthiobiotin and SA can form a complex that blocks the release of a drug or dye from the pores of a nanoparticle. To provide the SA-capped MSNs with another level of targeting capability and to further cap the pores and prevent drug/dye release, we performed additional functionalization with biotin-labeled HA. SEM showed that MSN-HA displayed a spherical morphology similar to that of MSN-NH_2 (Figure 2D), but the surface modification obscured the mesoporous structure of MSN-HA (Figure 2E). Zeta potential measurements showed that MSN-HA nanoparticles had a highly negative charge (−24.3 ± 0.5 mV) (Figure 2F) when compared with MSN-NH_2 (+38.4 ± 0.3 mV) and MSN-desthiobiotin (+38.2± 0.3 mV), confirming that HA had been successfully linked to the MSN surface. After Dox was loaded to generate MSN-HA/Dox, spectrophotometry revealed a drug-loading content of ~ 5% (w/w), which was comparable to that obtained in a previous study (28). In addition, as shown in Figure S3, MSN-HA/Dox showed low DPI value (0.157) and good dispersibility, indicating that potential aggregation of MSN-HA/Dox didn't occur and therefore the followed targeted therapeutic efficacy would not be affect. The successful loading of rhodamine B into the pores of MSN-HA was confirmed by fluorescence imaging, as shown in Figure S4.

MSN-HA nanoparticles show biotin- and HAase-dependent drug release

The K_d of biotin toward SA (K_d ~10^{-15} M) is about 10,000-fold higher than that of desthiobiotin (K_d ~10^{-11} M). In the context of our DDS, biotin will thus replace desthiobiotin within the cell, triggering drug release. To investigate the dual-stimulus-responsive release behavior of our designed MSN-HA DDS, we used biotin and HAase as triggers under conditions that mimicked the tumor microenvironment (pH 6.5). As shown in Figure 3, MSN/Dox exhibited higher Dox release in pH 6.5 solution when compared with MSN-HA/Dox. The cumulative release of Dox from MSN/Dox was more than 80% by 24 h. Under the same pH condition, MSN-HA/Dox released only ~ 12% of the loaded Dox, indicating that our use of desthiobiotin-SA complex and polysaccharide-HA yielded good capping. In the presence of biotin or HAase alone, the cumulative drug releases from MSN-HA/Dox were ~ 60% and 40%, respectively, at 24 h post-treatment. The cumulative drug release was further improved to ~ 70% in the presence of both biotin and HAase. This likely reflects the possible degradation of HA of MSN-HA/Dox by HAase and/or the displacement of desthiobiotin by biotin in co-treated cells compared to those treated with biotin alone. The

release profiles of Dox from MSN-HA/Dox under various stimulations in neutral buffer (pH 7.0) were also examined. We obtained release profiles similar to those observed under pH 6.5. Blood and healthy tissues are under neutral pH and express minimal biotin and HAase to trigger the release of Dox from MSN-HA/Dox. Therefore, our smart MSN-HA nanoparticles have very good capping efficacy, and do not release Dox until they reach the stimulating conditions (i.e., the cancer milieu) (Figure S5). Taken together, our results show that MSN-HA/Dox exhibits the highest drug release in the presence of both biotin and HAase under a pH that mimics the tumor microenvironment. Thus, our DDS shows great potential for tumor therapy.

MSN-HA can be taken up efficiently by Colon-26 and HT-29 cells through CD44 receptor mediated endocytosis

Efficient cellular uptake is a major requirement for the therapeutic efficacy of nanoparticles (3). To test the targeting specificity of MSN-HA, we evaluated the cellular uptake of MSN-HA/rhodamine B by Colon-26 cells and HT-29 cells. Membrane-localized CD44, which is known to be the main HA-binding receptor, is responsible for the interaction between HA and the surface of cancer cells (29). We incubated MSN-HA with Colon-26 and HT-29 cells at 37°C for 4 h with or without free HA. Subsequent confocal microscopy revealed that cells incubated with MSN-HA alone showed strong fluorescence of rhodamine B, both at the membrane and within the cells (Figure 4A–a, c). In the presence of free HA, in contrast, we observed less fluorescence from MSN-HA/rhodamine B in both Colon-26 and HT-29 cells (Figure 4A–b, d). This confirms that MSN-HA were subject to CD44-mediated endocytosis. The cellular uptake of MSN-HA/rhodamine B by Colon-26 and HT-29 cells was also assessed by flow cytometry, which revealed much higher fluorescence in HA-free cultures of Colon-26 (Figure 4B) and HT-29 cells (Figure 4C) than in their HA-treated counterparts. Together, our results are consistent with the idea that MSN-HA undergoes CD44 receptor-mediated endocytosis.

To confirm the involvement of receptor-mediated endocytosis, we performed a fluorescence-based co-localization study of MSN-HA/rhodamine B and FITC-labeled transferrin (Tf-FITC). Transferrin is internalized by receptor-mediated endocytosis *via* the formation of clathrin-coated pits, and is widely used as a tracker for clathrin-dependent endocytosis. Consistent with the results of our confocal microscopic and flow cytometric analyses, both Colon-26 and HT-29 cells showed high levels of co-localization between MSN-HA/rhodamine B (red color; Figure S6) and Tf-FITC (arrows, yellow color).

Evaluation the biocompatibility of MSN-HA both *in vitro* and *in vivo*

For a potential DDS, biocompatibility is a key issue that should be investigated. To assess the biocompatibility of MSN-HA, we first used MTT assays to quantify the viability of cells treated with different concentrations of MSN and MSN-HA. Colon-26 and HT-29 cells treated with MSN-HA showed higher cell viability than those treated with the same concentrations of MSN at up to the highest tested dose of 200 μg/ml (Figure S7A and B), indicating that HA modification improved the biocompatibility of MSN. An ATPLite assay, which quantitatively measures cell proliferation, confirmed these results (Figure S7C and D). These results indicate that MSN-HA has good biocompatibility *in vitro*.

Next, we explored the biocompatibility of MSN-HA *in vivo*. Intravenous i.v. injection of mice with MSN-HA (1 mg/100 μl) daily for 7 days did not trigger any change in the weights/body weights of the heart, liver, spleen, lung, or kidney (Figure S8A). Histological analysis of H&E-stained tissue sections did not find any clear evidence of organ damage in the MSN-HA group compared with the control group. The liver hepatocytes appeared normal; no myocardial fibrillary loss or vacuolation was observed in the heart; no pulmonary fibrosis was detected in lung samples; and no necrosis was observed in any analyzed samples (Figure S8B). We also failed to observe any significant increase in the indicators of liver injury, alanine aminotransferase (ALT) or aspartate aminotransferase (AST), in the MSN-HA group compared with the control group (Figure S8C). Collectively, these findings indicate that MSN-HA exhibits higher biocompatibility both *in vitro* and *in vivo,* and therefore should be useful as a safe drug-delivery platform.

Nuclear transport of Dox and subsequent cell apoptosis

Research showed that Dox can diffuse into nuclei, where it interacts with DNA molecules (30). As shown in Figure S9, free Dox or MSN-HA/Dox-released Dox was transported into nuclei after 8 h incubation, indicating that MSN-HA/Dox can successfully be taken up and deliver Dox into the nucleus to exert its function.

To compare the apoptosis induced by free Dox and MSN-HA/Dox, we used Annexin V-FITC and PI double staining to examine treated Colon-26 and HT-29 cells. Fluorescence microscopy revealed that free Dox- and MSN-HA/Dox-treated Colon-26 cells showed positive staining for both Annexin V-FITC and PI (Figure 5A), whereas no such signal was detected from untreated control cells. Flow cytometry-based quantification revealed apoptotic cell populations of 90.8±5.5%, 41.8±9.2%, and 3.2±2.1% in MSN-HA/Dox-treated, free Dox-treated, and control cells, respectively (Figure 5B and C). Similar results were obtained in HT-29 cells, which exhibited apoptotic populations of 90.7±1.5%, 50.2±5.6%, and 1.1±0.9%, respectively (Figure S10). We also compared apoptosis using 3-(4,5-dimethylthiazol-2-yl)-2,5-diphenyltetrazolium bromide (MTT) assays. As shown in Figure 5D and E, MSN-HA/Dox induced more cell apoptosis than free Dox at all tested concentrations (0.5, 1.0, 2.0, and 5.0 μg/ml Dox) in both Colon-26 and HT-29 cells. These results confirmed that MSN-HA/Dox has a higher therapeutic effect than free Dox. Consequently, MSN-HA/Dox could improve the therapeutic effect of Dox and might serve as a good DDS.

MSN-HA shows relatively little non-specific interaction with proteins, blood cells and macrophages

After a nanoparticle enters the circulation, the first biological event is the adsorption of the abundant plasma proteins onto to the nanoparticle surface (31). This would be expected to change the surface characteristics of a nanoparticle-based DDS and impact its delivery efficiency *in vivo*. To investigate the interaction of MSN-SA with such proteins, we followed previous studies by using bovine serum albumin (BSA) (15), which is a major serum protein often found in the protein corona of nanoparticles. As shown in Figure S11A, significantly less BSA was absorbed by MSN-HA compared to MSN at both 12 h and 24 h. This suggests

that the surface-bound HA prevents proteins from adsorbing into the MSN, which could prolong the circulation time of our DDS in the blood (32).

In blood, the hemolysis by nanoparticles seriously limits the *in vivo* application of nanoparticle-based DDS (33, 34). In our studies, however, while Triton X-100 (positive control) achieved 100% hemolysis, MSN-HA did not trigger hemolysis at concentrations up to 1 mg/ml (Figure S11B). This suggests that i.v.-administered MSN-HA could be nontoxic towards erythrocytes.

When nanoparticles enter a host, they firstly interact with macrophages to trigger immune responses, such as inflammation. Prominent inflammatory mediators, IL-6, IL-1β and TNF-α, are typically used as markers of an acute macrophage-related inflammatory response (35). As shown in Figure S12A–C, the mRNA levels of IL-6, IL-1β and TNF-α were significantly lower in MSN-HA-treated RAW 264.7 cells (a macrophage cell line) than in MSN-treated cells. To further investigate the immunological effect of MSN-HA/Dox *in vivo*, we subjected mice to single-dose injections of MSN-HA/Dox, and obtained sera at 24 h and 48 h post-injection. As shown in Figure S12D–F, the protein concentrations of IL-6, IL-1β and TNF-α were not significantly different between MSN-HA/Dox-injected and control mice at 24 h and 48 h, indicating that HA capping of MSN reduced the likelihood of triggering a macrophage-induced inflammatory response. These observations reflect the improvement of the biocompatibility of MSN via the conjugation of HA, thereby reducing the inflammatory response triggered by our MSN-HA delivery system.

Anti-tumor effects of MSN-HA/Dox *in vivo*

To evaluate the anti-tumor effects of MSN-HA/Dox *in vivo*, we established a Colon-26 xenograft tumor model in athymic BALB/c nu/nu mice. The tumor-bearing mice were randomly divided into four groups and i.v. injected with saline, MSN-HA, free Dox, or MSN-HA/Dox. As shown in Figure 6A, visual observations indicated that the MSN-HA/Dox-treated mice showed the most efficient reduction of tumor size. The saline- and MSN-HA-treated control groups exhibited similar tumor volumes at the end of the experiment (Figure 6B), whereas the free Dox-treated group showed slightly decreased tumor growth compared with the control groups (Figure 6B). At the end of the experiment, tumor weights were compared. As shown in Figure 6C, the MSN-HA/Dox-treated group showed the lowest tumor weight, which was significantly lower than that of the free Dox-treated group. The saline- and MSN-HA-treated control groups displayed similar tumor weights, indicating similar tumor growth.

These findings, which are consistent with the results of our *in vitro* apoptosis assays, indicate that MSN-HA/Dox shows better tumor growth inhibition than free Dox *in vivo*. This may reflect that free Dox quickly diffuses into tissues and organs following i.v. injection (31), potentially affecting normal tissues and decreasing the amount of free drug that would reach the tumor site. Moreover, free Dox has a short half-life *in vivo* and is quickly cleared from the body (36).

To explore the mechanism underlying the tumor growth inhibition conferred by our DDS, we performed TUNEL (terminal deoxynucleotidyl transferase dUTP nick-end labeling)

apoptosis assays. As shown in Figure 6D, few TUNEL-positive apoptotic cells (green dots) were detected in tumor sections from the saline- and MSN-HA-treated groups, providing additional evidence that MSN-HA shows good biocompatibility *in vivo*. In contrast, tumor tissues from the MSN-HA/Dox-treated group showed the most severe apoptosis among the different groups, indicating that MSN-HA/Dox inhibits the growth of solid tumor model by inducing apoptosis.

To further confirm the improved therapeutic efficacy of MSN-HA/Dox, we performed histological analysis of tumor tissues. H&E staining and subsequent analysis (Figure S13) revealed that sections from the MSN-HA/Dox-treated group harbored significantly fewer cancerous cells than those from the saline-, MSN-HA- and free Dox-treated groups.

To investigate the potential side effects of MSN-HA/Dox, we performed histological examinations of major organs (heart, liver, spleen, lung and kidney) at the end of the experiment. As shown in Figure 7, mice of the control and MSN-HA/Dox groups did not show any noticeable signs of tissue or cellular damage in the examined tissues (e.g., myocardial fibrillar loss or vacuolation in the heart; edema, ballooning and/or degeneration of hepatocytes; increased numbers of granulocytes in the spleen; tubular vacuolization or tubular dilation with hemorrhagic areas in the kidney; or increased alveolar wall thickness or cellular infiltration in the lung). In contrast, free Dox induced typical myocardial damage with intensive vacuolization and myofibril loss (Figure 7, blue circles).

To investigate time-dependent bio-distribution of our drug delivery system, we administered a single dose of MSN-HA/near-infrared dye (DiL) to mice via intravenous injection. No post-injection abnormality was observed in the eating, drinking, grooming, activity, exploratory behavior, urination, or neurological status of treated mice. At 4 h, 24 h, and 7 d post-injection, mice were sacrificed and the DiL contents were measured in different organs (heart, liver, spleen, lung and kidney) using an IVIS *in vivo* imaging system. As shown in Figure S14, MSN-HA/DiL was predominately found in organs of the reticuloendothelial system (liver and spleen) at 4 h and 24 h post-injection. The dye was noticeably cleared from the body within one week. This biodistribution reflects that the protective HA layer on the surface of the MSN nanoparticles prevented this drug delivery system from being recognized and engulfed by phagocytes of the liver and spleen, thereby reducing the cellular uptake by liver and spleen. These results suggest that MSN-HA/Dox could have a low toxicity to the body, and could thus be suitable for use as a real anticancer system *in vivo*. Our findings in this regard are consistent with those of the previous studies (16, 31, 37).

Based on the results presented in this report, we conclude that our biotin/HAase dual-responsive mesoporous silica drug delivery system (MSN-HA/Dox) exhibits better selective anti-tumor effects against solid tumors than free Dox. Mechanistically, these effects reflect that: (1) the HA on the surface of MSN-HA/Dox uses active targeting to improve the selective delivery of the loaded drug to tumor tissues; (2) the capping of the pores alleviates the premature release of highly toxic anti-cancer drugs during the delivery process; and (3) extracellular matrix-localized HAase and intracellular biotin both trigger the release of the encapsulated Dox, improving its anti-proliferative activity in a solid cancer. Since the zeta

potential of MSN-HA/Dox was highly negative, it is reasonable to believe that the nanoparticles escape from the endosome to interact with biotin in the cytoplasm (23).

In conclusion, we herein designed and constructed a biotin and hyaluronidase dual-responsive DDS (MSN-HA/Dox) for a targeted therapeutic drug delivery *in vitro* and *in vivo*. Desthiobiotin-modified MSN was used as the initial carrier to load Dox. The polysaccharide, hyaluronic acid, was grafted onto the MSN surface via the biotin-streptavidin interaction to serve as a targeting moiety. The pores of this delivery system were capped by desthiobiotin/streptavidin complexes and HA to eliminate the premature drug leakage. Following uptake of the nanoparticles by target cells, HAase in the extracellular matrix and biotin in the cytoplasm opened the pores for controlled intracellular release of the entrapped drug. MSN-HA/Dox triggered enhanced apoptosis among cancer cells *in vitro* and conferred better anti-tumor effects *in vivo* compared to the free drug. Our findings suggest that this novel DDS may hold promise for efficient tumor therapy.

Supplementary Material

Refer to Web version on PubMed Central for supplementary material.

Acknowledgments

Financial support: This work was funded by the National Institutes of Health of Diabetes and Digestive and Kidney (RO1-DK-071594 to D.M).

References

1. Thun MJ, DeLancey JO, Center MM, Jemal A, Ward EM. The global burden of cancer: priorities for prevention. Carcinogenesis. 2010; 31:100–10. [PubMed: 19934210]
2. Brigger I, Dubernet C, Couvreur P. Nanoparticles in cancer therapy and diagnosis. Adv Drug Deliv Rev. 2012; 64:24–36.
3. Xiao B, Zhang M, Viennois E, Zhang Y, Wei N, Baker MT, et al. Inhibition of MDR1 gene expression and enhancing cellular uptake for effective colon cancer treatment using dual-surface-functionalized nanoparticles. Biomaterials. 2015; 48:147–60. [PubMed: 25701040]
4. Wei T, Liu J, Ma H, Cheng Q, Huang Y, Zhao J, et al. Functionalized nanoscale micelles improve drug delivery for cancer therapy in vitro and in vivo. Nano Lett. 2013; 13:2528–34. [PubMed: 23634882]
5. Kanamala M, Wilson WR, Yang M, Palmer BD, Wu Z. Mechanisms and biomaterials in pH-responsive tumour targeted drug delivery: A review. Biomaterials. 2016; 85:152–67. [PubMed: 26871891]
6. Baeza A, Colilla M, Vallet-Regí M. Advances in mesoporous silica nanoparticles for targeted stimuli-responsive drug delivery. Expert Opin Drug Deliv. 2015; 12:319–37. [PubMed: 25421898]
7. Murata M, Narahara S, Kawano T, Hamano N, Piao JS, Kang J-H, et al. Design and function of engineered protein nanocages as a drug delivery system for targeting pancreatic cancer cells via neuropilin-1. Mol Pharm. 2015; 12:1422–30. [PubMed: 25811429]
8. Prabhakar U, Maeda H, Jain RK, Sevick-Muraca EM, Zamboni W, Farokhzad OC, et al. Challenges and key considerations of the enhanced permeability and retention effect for nanomedicine drug delivery in oncology. Cancer Res. 2013; 73:2412–17. [PubMed: 23423979]
9. Keereweer S, Mol IM, Kerrebijn JD, Van Driel PB, Xie B, de Jong B, et al. Targeting integrins and enhanced permeability and retention (EPR) effect for optical imaging of oral cancer. J Surg Oncol. 2012; 105:714–18. [PubMed: 21952950]

10. Doleschel D, Rix A, Arns S, Palmowski K, Gremse F, Merkle R, et al. Erythropoietin improves the accumulation and therapeutic effects of carboplatin by enhancing tumor vascularization and perfusion. Theranostics. 2015; 5:905. [PubMed: 26000061]
11. Salvati A, Pitek AS, Monopoli MP, Prapainop K, Bombelli FB, Hristov DR, et al. Transferrin-functionalized nanoparticles lose their targeting capabilities when a biomolecule corona adsorbs on the surface. Nat Nanotechnol. 2013; 8:137–43. [PubMed: 23334168]
12. Weiser JR, Saltzman WM. Controlled release for local delivery of drugs: barriers and models. J Control Release. 2014; 190:664–73. [PubMed: 24801251]
13. Yin Q, Shen J, Zhang Z, Yu H, Li Y. Reversal of multidrug resistance by stimuli-responsive drug delivery systems for therapy of tumor. Adv Drug Deliv Rev. 2013; 65:1699–715. [PubMed: 23611952]
14. Zhao Q, Liu J, Zhu W, Sun C, Di D, Zhang Y, et al. Dual-stimuli responsive hyaluronic acid-conjugated mesoporous silica for targeted delivery to CD44-overexpressing cancer cells. Acta biomater. 2015; 23:147–56. [PubMed: 25985912]
15. Zhao Q, Geng H, Wang Y, Gao Y, Huang J, Wang Y, et al. Hyaluronic acid oligosaccharide modified redox-responsive mesoporous silica nanoparticles for targeted drug delivery. ACS Appl Mater Interfaces. 2014; 6:20290–99. [PubMed: 25311422]
16. Chen Y, Ai K, Liu J, Sun G, Yin Q, Lu L. Multifunctional envelope-type mesoporous silica nanoparticles for pH-responsive drug delivery and magnetic resonance imaging. Biomaterials. 2015; 60:111–20. [PubMed: 25988726]
17. Aznar E, Villalonga R, Giménez C, Sancenón F, Marcos MD, Martínez-Máñez R, et al. Glucose-triggered release using enzyme-gated mesoporous silica nanoparticles. Chem Commun. 2013; 49:6391–93.
18. Wang Y, Zhao Q, Han N, Bai L, Li J, Liu J, et al. Mesoporous silica nanoparticles in drug delivery and biomedical applications. Nanomedicine. 2015; 11:313–27. [PubMed: 25461284]
19. Yang X, Liu X, Liu Z, Pu F, Ren J, Qu X. Near-Infrared Light-Triggered, Targeted Drug Delivery to Cancer Cells by Aptamer Gated Nanovehicles. Adv Mater. 2012; 24:2890–95. [PubMed: 22539076]
20. Shang L, Bian T, Zhang B, Zhang D, Wu LZ, Tung CH, et al. Graphene-supported ultrafine metal nanoparticles encapsulated by mesoporous silica: robust catalysts for oxidation and reduction reactions. Angew Chem Int Ed. 2014; 53:250–54.
21. Choi KY, Yoon HY, Kim J-H, Bae SM, Park R-W, Kang YM, et al. Smart nanocarrier based on PEGylated hyaluronic acid for cancer therapy. ACS Nano. 2011; 5:8591–99. [PubMed: 21967065]
22. Dosio F, Arpicco S, Stella B, Fattal E. Hyaluronic acid for anticancer drug and nucleic acid delivery. Adv Drug Deliv Rev. 2016; 97:204–36. [PubMed: 26592477]
23. Li L-L, Xie M, Wang J, Li X, Wang C, Yuan Q, et al. A vitamin-responsive mesoporous nanocarrier with DNA aptamer-mediated cell targeting. Chem Commun. 2013; 49:5823–25.
24. Russell-Jones G, McTavish K, McEwan J, Rice J, Nowotnik D. Vitamin-mediated targeting as a potential mechanism to increase drug uptake by tumours. J Inorg Biochem. 2004; 98:1625–33. [PubMed: 15458825]
25. Chivers CE, Crozat E, Chu C, Moy VT, Sherratt DJ, Howarth M. A streptavidin variant with slower biotin dissociation and increased mechanostability. Nat Methods. 2010; 7:391–93. [PubMed: 20383133]
26. Zhang J, Yuan Z-F, Wang Y, Chen W-H, Luo G-F, Cheng S-X, et al. Multifunctional envelope-type mesoporous silica nanoparticles for tumor-triggered targeting drug delivery. J Am Chem Soc. 2013; 135:5068–73. [PubMed: 23464924]
27. Muhammad F, Guo M, Qi W, Sun F, Wang A, Guo Y, et al. pH-triggered controlled drug release from mesoporous silica nanoparticles via intracelluar dissolution of ZnO nanolids. J Am Chem Soc. 2011; 133:8778–81. [PubMed: 21574653]
28. Liu J, Zhang B, Luo Z, Ding X, Li J, Dai L, et al. Enzyme responsive mesoporous silica nanoparticles for targeted tumor therapy in vitro and in vivo. Nanoscale. 2015; 7:3614–26. [PubMed: 25633047]
29. Götte M, Yip GW. Heparanase, hyaluronan, and CD44 in cancers: a breast carcinoma perspective. Cancer Res. 2006; 66:10233–37. [PubMed: 17079438]

30. Sui M, Liu W, Shen Y. Nuclear drug delivery for cancer chemotherapy. J Control Release. 2011; 155:227–36. [PubMed: 21846484]

31. Liu J, Luo Z, Zhang J, Luo T, Zhou J, Zhao X, et al. Hollow mesoporous silica nanoparticles facilitated drug delivery via cascade pH stimuli in tumor microenvironment for tumor therapy. Biomaterials. 2016; 83:51–65. [PubMed: 26773665]

32. Yoo J-W, Chambers E, Mitragotri S. Factors that control the circulation time of nanoparticles in blood: challenges, solutions and future prospects. Curr Pharm Des. 2010; 16:2298–307. [PubMed: 20618151]

33. Lin Y-S, Haynes CL. Impacts of mesoporous silica nanoparticle size, pore ordering, and pore integrity on hemolytic activity. J Am Chem Soc. 2010; 132:4834–42. [PubMed: 20230032]

34. Chen LQ, Fang L, Ling J, Ding CZ, Kang B, Huang CZ. Nanotoxicity of silver nanoparticles to red blood cells: size dependent adsorption, uptake, and hemolytic activity. Chem Res Toxicol. 2015; 28:501–09. [PubMed: 25602487]

35. Zhang M, Viennois E, Prasad M, Zhang Y, Wang L, Zhang Z, et al. Edible ginger-derived nanoparticles: A novel therapeutic approach for the prevention and treatment of inflammatory bowel disease and colitis-associated cancer. Biomaterials. 2016; 101:321–40. [PubMed: 27318094]

36. Vu-Quang H, Vinding MS, Nielsen T, Ullisch MG, Nielsen NC, Kjems J. Theranostic tumor targeted nanoparticles combining drug delivery with dual near infrared and 19 F magnetic resonance imaging modalities. Nanomedicine. 2016; 12:1873–84. [PubMed: 27133191]

37. He Q, Zhang Z, Gao F, Li Y, Shi J. In vivo biodistribution and urinary excretion of mesoporous silica nanoparticles: effects of particle size and PEGylation. Small. 2011; 7:271–80. [PubMed: 21213393]

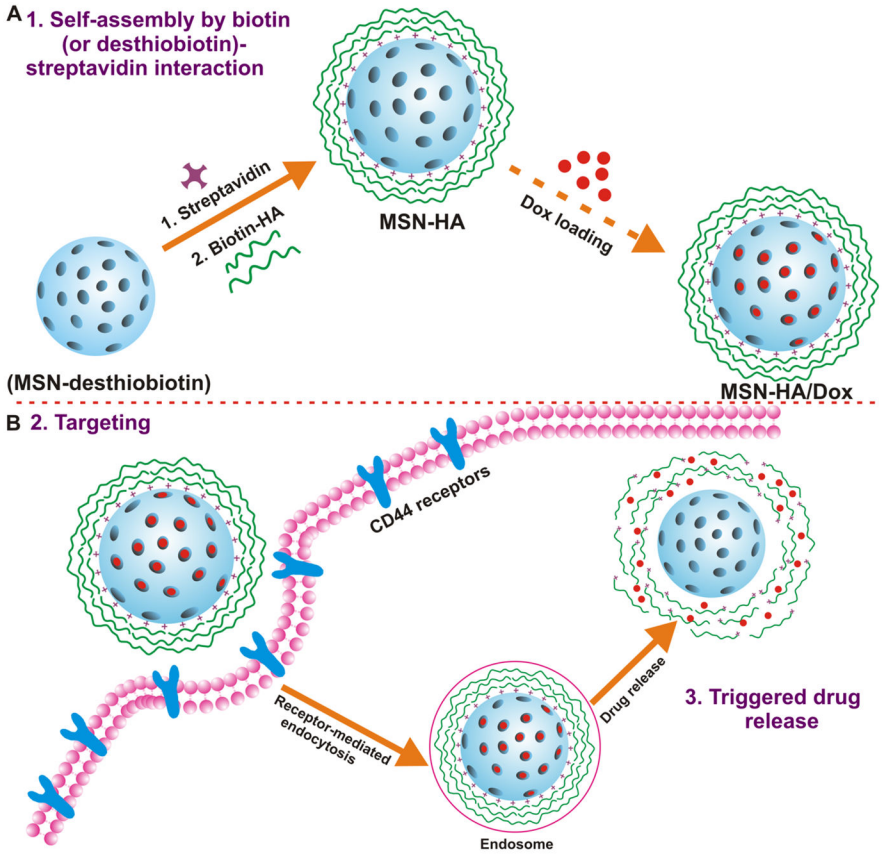

Figure 1. Schematic diagram to describe MSN-HA nanoparticles mediated delivery of the therapeutic drug, doxorubicin (Dox), to cancer cells

A. Drug loading steps to yield MSN-HA/Dox delivery system. Propylamine functionalized silica (MSN-NH_2) was first modified with desthiobiotin to obtain MSN-desthiobiotin, then by employing biotin (or desthiobiotin)-SA interaction, SA and biotinylated HA were self-assembled on the external surface of MSN to yield MSN-HA. Optionally, therapeutic drug, Dox, was able to load to obtain MSN-HA/Dox. **B.** Schematic illustration of the CD44-receptor-mediated endocytosis and triggering of drug release in tumor cells. MSN-HA/Dox were taken up by cancer cell via receptor-mediated endocytosis (HA-CD44 interaction), then loaded Dox was release from the pore of MSN by the triggering of HAase and intracellular biotin.

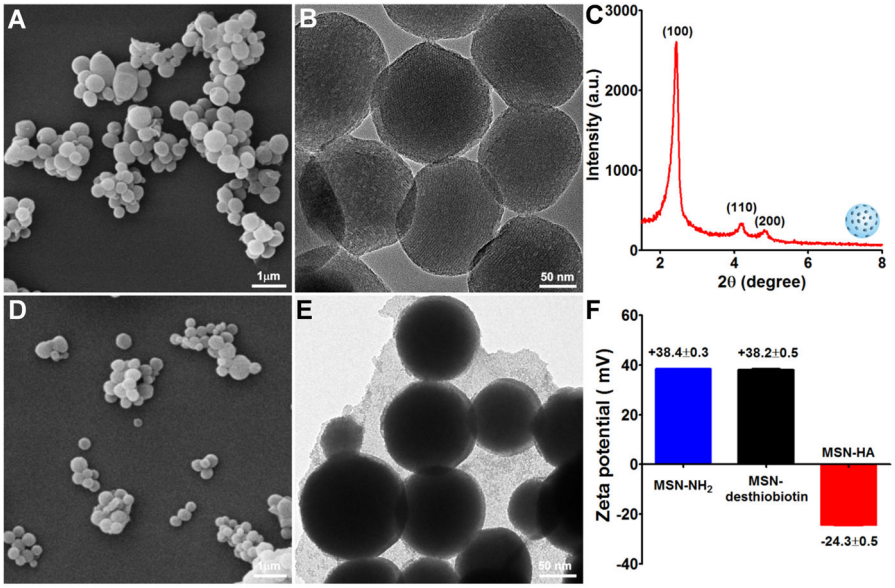

Figure 2. Characterization of MSN-NH_2 and MSN-HA nanoparticles

A. SEM images were performed to characterize MSN-NH_2 nanoparticles, scale bar: 1 μm. **B.** TEM images were performed to characterize MSN-NH_2 nanoparticles, scale bar: 50 nm. **C.** Small-angle power X-ray diffraction was employed to characterize the structure of MSN-NH_2. The high ordered lattice array indicated MSN-NH_2 has a uniform and well-defined mesostructure. **D.** SEM images of MSN-HA, scale bar: 1 μm. **E.** TEM images of MSN-HA, scale bar: 50 nm. **F.** Zeta potentials of MSN-NH_2, MSN-desthiobiotin, and MSN-HA were measured. MSN-NH_2 and MSN-desthiobiotin showed a positive surface charge, after grafting HA, surface charge was changed to negative, indicating the successful link of HA, (n=3).

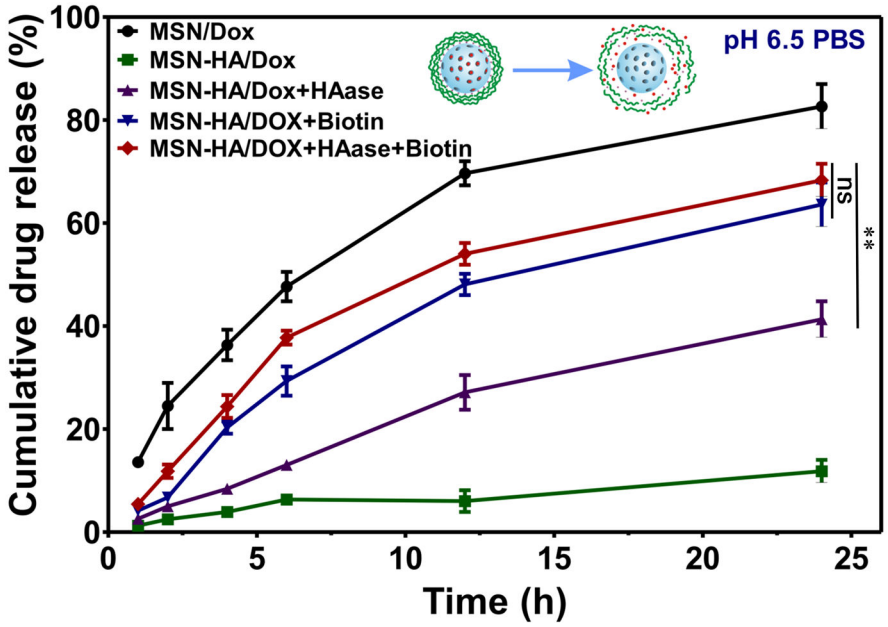

Figure 3.

The biotin- and HAase-responsive release profiles of Dox were evaluated. Drug release under pH 6.5 was conducted to mimic the condition of tumor microenvironment. Under different stimulus condition, biotin (2 μM), HAase (150U/ml) or both were added to MSN-HA/Dox solution; as a control, MSN-Dox was employed. At specified time points (1, 2, 4, 6, 12, and 24 h), cumulative drug release were measured and compared, (n=3).

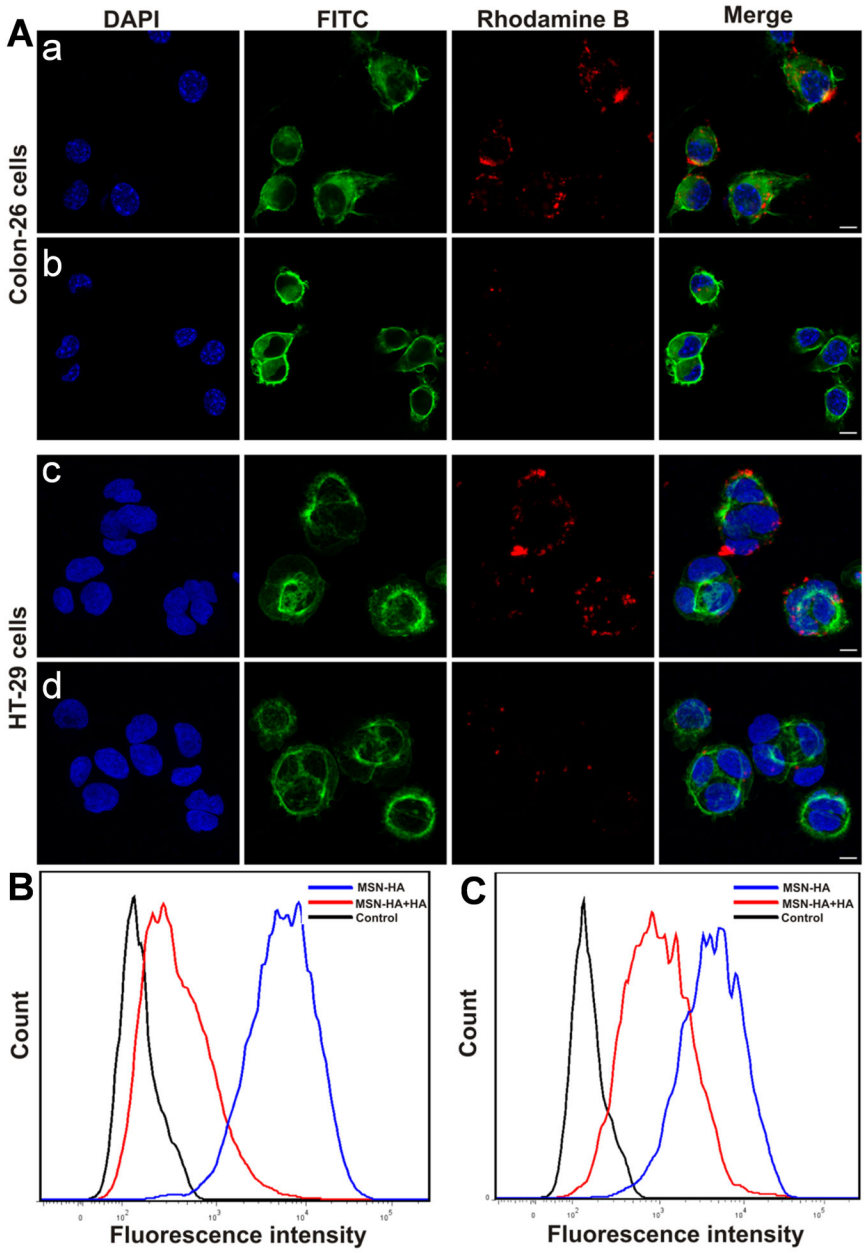

Figure 4.

Endocytosis pathway of MSN-HA taken up by Colon-26 and HT-26 cells was investigated. **A.** Confocal microscopic images show: a, Colon-26 cells treated with MSN-HA in the absence of HA; b, Colon-26 cells treated with MSN-HA in the presence of HA (2mg/ml); c, HT-29 cells treated with MSN-HA in the absence of HA; d, HT-29 cells treated with MSN-HA in the presence of HA (2mg/ml). Blue channel: DAPI; Green channel: FITC; Red channel: the fluorescence of rhodamine B. The fluorescence intensities of rhodamine B-labeled MSN-HA applied with or without HA were quantified by flow cytometry. **B.** Colon-26 cells. **C**. HT-29 cells. (n = 5). Scale bar: 20 μm.

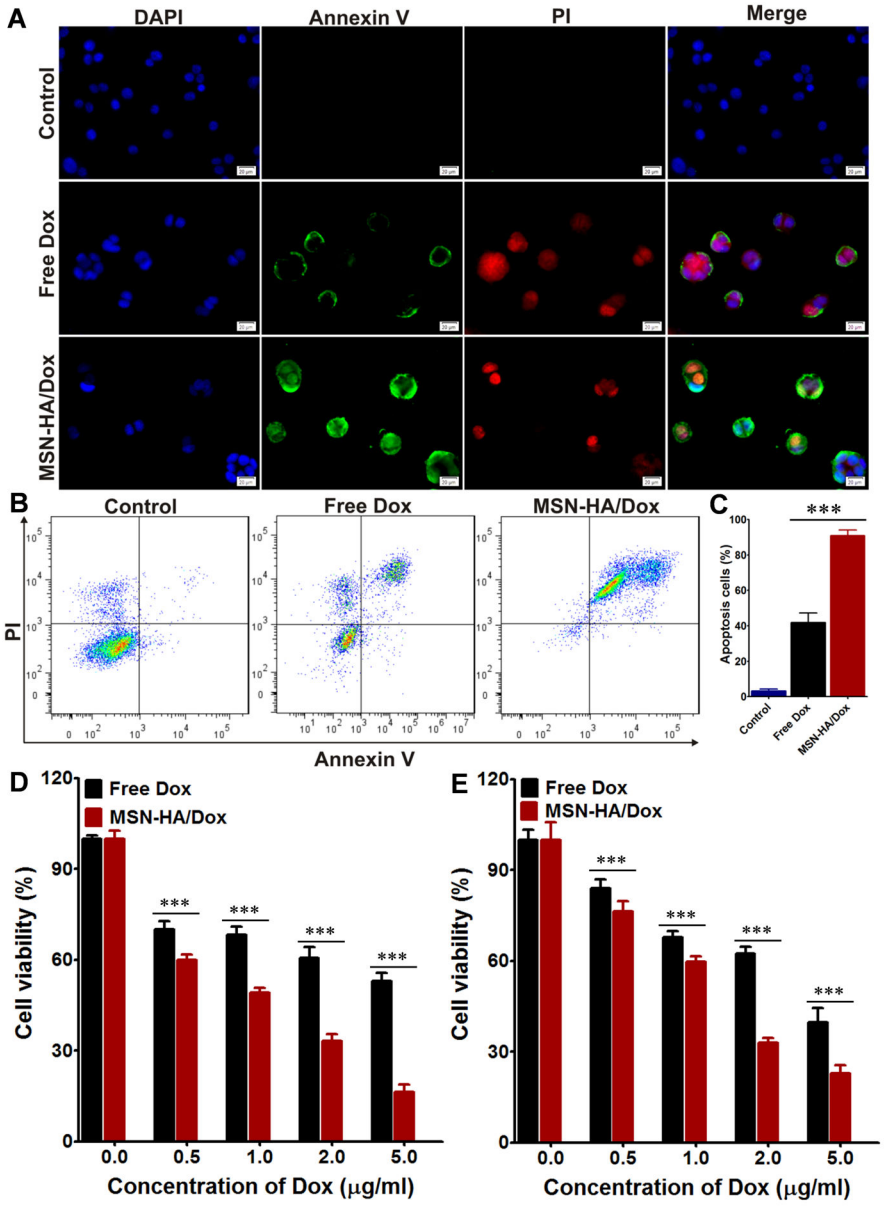

Figure 5.

Evaluation the apoptosis induced by MSN-HA/Dox *in vitro*. **A.** Fluorescence imaging of Colon-26 cells treated with free Dox or MSN-HA/Dox for 8 h and then co-stained with Annexin V-FTIC and PI. Scale bar: 20 μm. **B.** Flow cytometric analysis of apoptosis in Colon-26 cells treated with free Dox or MSN-HA/Dox for 8 h. **C.** Quantification of the Annexin V-FTIC/PI-positive apoptotic cells from panel B. Data are from three independent experiments. **D.** The apoptotic effects of free Dox and MSN-HA/Dox in Colon-26 cells were assessed by MTT assay, (n=5). **E.** The apoptotic effects of free Dox and MSN-HA/Dox in HT-29 cells were assessed by MTT assay, (n=5), ***$p < 0.001$.

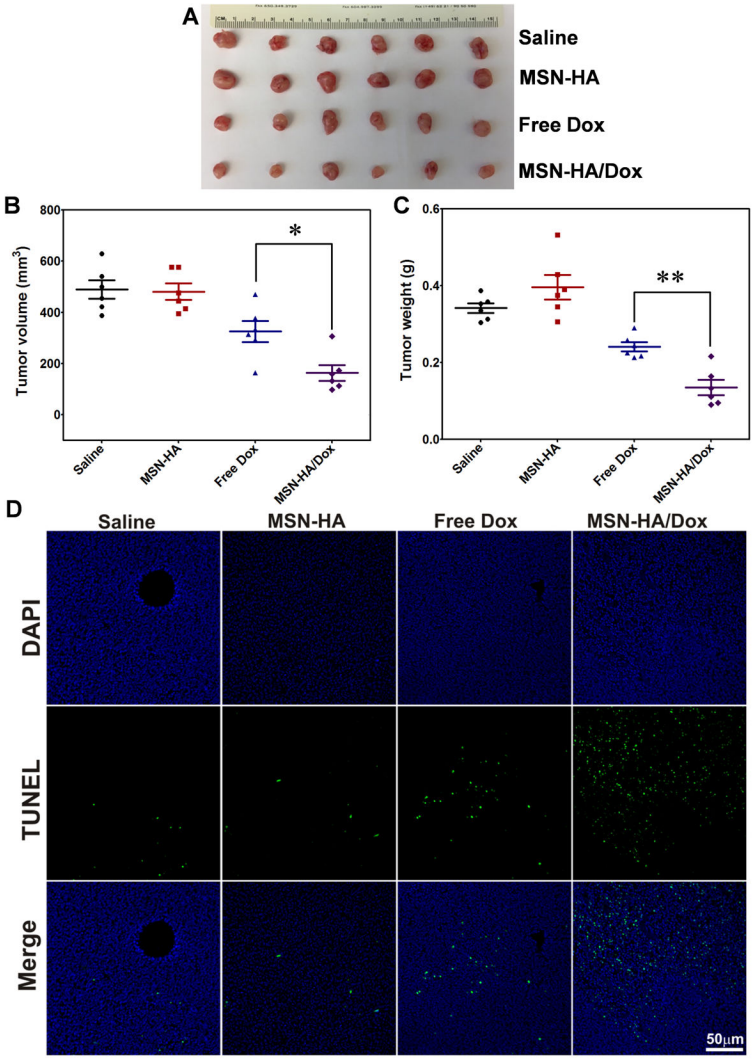

Figure 6.

Effects of MSN-HA/Dox against Colon-26 xenograft tumors were evaluated *in vivo*. **A.** Representative Photos of tumor tissues obtained from tumor-bearing mice treated for 18 days with saline (control), MSN-HA, free Dox, or MSN-HA/Dox, (n=6). **B.** Tumor volumes were measured at the end of the experiment (n=6). **C.** Tumor weights were measured at the end of the experiment (n=6). **D.** TUNEL staining was used to examine apoptosis in tumor sections (green, TUNEL positive cells; blue, cell nuclei), (n=4). Scale bar: 50 μm; *$p < 0.05$ and **$p < 0.01$.

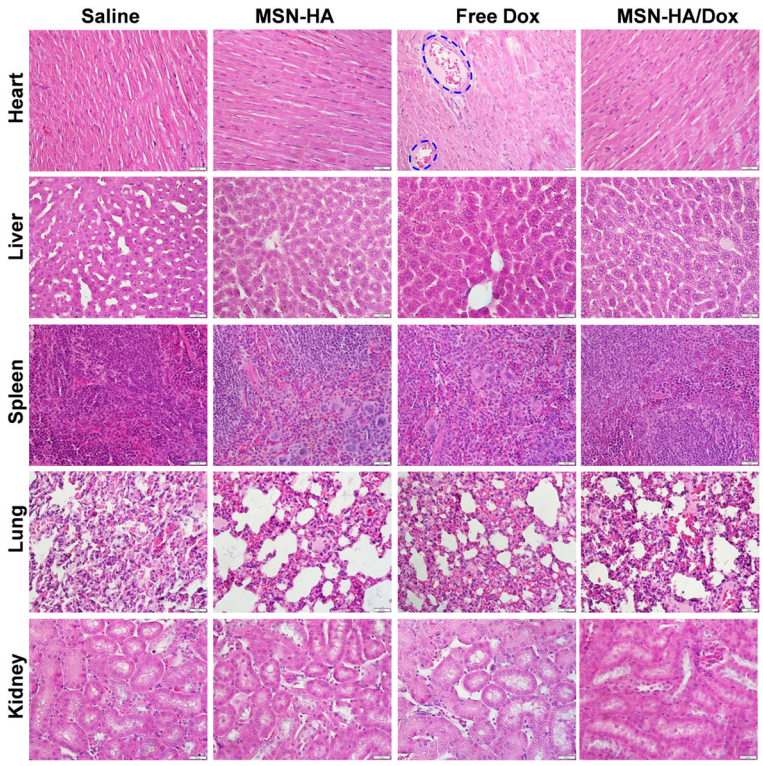

Figure 7.

The major organs of tumor-bearing mice treated with saline, MSN-HA, free Dox, or MSN-HA/Dox were subjected to histological examination. Heart samples of free Dox-treated mice show intensive vacuolization and myofibril loss (as indicated). Scale bar: 20 μm.